

Stabilizing the free spectral range of a large ring laser

Jannik Zenner and Simon Stellmer*

Physikalisches Institut, Universität Bonn, Nussallee 12, 53115 Bonn, Germany

Karl Ulrich Schreiber

*Research Unit Satellite Geodesy, Technical University of Munich, 80333 Munich, Germany and
School of Physical Sciences, University of Canterbury, Christchurch 8140, New Zealand*

(Dated: November 27, 2024)

Large ring lasers employed in geodesy and fundamental physics require stability of the perimeter at or below the parts-per-billion level. We present two complementary approaches to actively control the perimeter length of such ring lasers, reaching a relative length stability of 4×10^{-10} . These methods can readily be implemented and bring the stability of heterolithic devices on par with monolithic designs.

I. INTRODUCTION

The winter 2024/25 marks the centennial of the famous Michelson-Gale-Pearson experiment [1, 2]. On an open field near Chicago, A. A. Michelson and his co-workers had installed a large rectangular interferometer, with arm lengths measuring 612 by 339 meters. Two light fields propagating in opposite directions along the contour will acquire a phase shift proportional to the rotation rate of the setup, known today by one of the pioneers in optical rotation measurements, G. Sagnac [3]. The crew of 1924 observed a fringe shift of 0.270λ when comparing the interference pattern of the large ring with a zero-area reference setup. This observation agreed to within 2% with the calculated value from the Earth rotation rate. This hallmark experiment was, although unintended, the first measurement of Earth rotation based on the Sagnac effect, and one of the first tests of special relativity in the limit of small velocities.

Today, various experiments around the world are targeted at highly sensitive rotation measurements using large, meter-sized ring resonators in the fields of geodesy [4, 5], seismology [6, 7], and fundamental physics [8, 9]. Some of these instruments are contemporary versions of the 1924 setup, so-called passive ring resonators with an external laser feeding two counter-propagating resonator modes [10–12]. Alternatively, the laser medium, usually a helium-neon gas, may be placed inside the ring resonator, forming a ring laser. To our knowledge, only two of these instruments are quasi-monolithic structures with very small mechanical instabilities: the C-II ring in Canterbury (New Zealand), which was the first ring laser to measure low frequency geophysical signals beyond the rotation of Earth [13], and the G ring in Wettzell (Germany), which currently is the frontrunner in terms of sensitivity and stability [14]. All heterolithic devices will benefit from an active stabilization of the resonator perimeter. Such approaches have been demonstrated for passive ring resonators [15], but not for ring lasers.

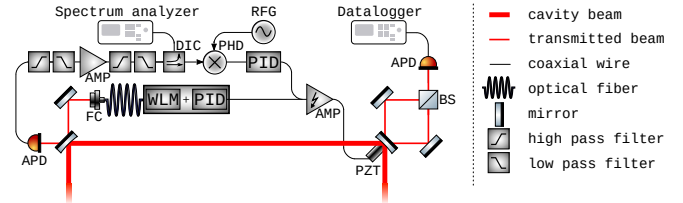


Figure 1. Schematic view of the setup to stabilize the perimeter of the ring laser cavity using either the *absolute frequency lock* or *FSR phase lock* method (left-hand side corner) and to measure the Sagnac frequency (right-hand side corner). Abbreviations: AMP *radio frequency amplifier*, APD *avalanche photodetector*, BS *beamsplitter*, DIC *directional coupler*, FC *fiber coupler*, PHD *phase detector*, PID *proportional-integral-derivative controller*, PZT *piezo actuator*, RFG *radio frequency generator*, WLM *wavelength meter*.

Here, we present two approaches that allow stabilization of the perimeter of a ring laser to a few nanometer, equivalent to a relative instability in the 10^{-10} range.

Consider a ring-shaped optical resonator with perimeter P and enclosed area A , rotating at a rate Ω . The Sagnac frequency of two counter-propagating modes of the same longitudinal mode index m reads

$$\delta f = \frac{4A}{\lambda P} \Omega \sin \theta, \quad (1)$$

where λ is the wavelength of the light and θ is the projection angle of the surface vector onto the rotation vector. The dimensionless pre-factor $4A/\lambda P$ is called the scale factor. Another important quantity is the free spectral range (FSR), which is the frequency splitting between adjacent longitudinal modes of the the resonator, $f_{\text{FSR}} = c/P$. The FSR is directly proportional to the ring perimeter P , and we will present two approaches to stabilize the perimeter through stabilization of the FSR.

II. SETUP

The setup is based on a square ring laser with an side length of about 3.5 m, the details of which have been

* stellmer@uni-bonn.de

described elsewhere [16, 17]. The resonator is formed by four mirrors with a radius of curvature of 4 m and has a finesse of about 40,000. The ring laser usually operates at an absolute frequency of 473 612 110(2) MHz, the free spectral range is 21 423 199.0(1) Hz and the inferred mode index, corrected for various small systematics detailed in Ref. [18], is $m = 22107440.0(0.4)$. The measured Sagnac frequency of $\delta f = 311.65$ Hz is in very good agreement with expectations from the known Earth rotation rate Ω_E and the latitude of the ring laser, $\theta' = 50^\circ 43' 41.9''$ N.

The technical setup is shown in Fig. 1. At one of the ring cavity mirrors, a 3.5-ppm fraction of the two counter-propagating light fields is coupled out of the cavity, passes through anti-reflection coated vacuum windows, and is superimposed on a non-polarizing 50:50 beamsplitter. The two path lengths between cavity mirror and beamsplitter are equal to within a millimeter. The signal is measured with an avalanche photodetector and digitized with a data logger. The Sagnac beat signal has a contrast greater than 95%.

The cavity mirror holder of that same corner is fixed to a multilayer stack piezo actuator with a total motion range of 89 μm oriented orthogonal to the mirror surface, allowing for a perimeter variation of up to $\Delta P = 126$ μm and a possible shift of the FSR of up to $\Delta f_{\text{FSR}} = 193$ Hz.

To stabilize the perimeter of the ring laser cavity, the piezo is steered according to one of two parameters detected at the left-hand side of Fig. 1. The light is either coupled into a fiber, which is then used to perform an *absolute frequency lock*, or it is detected by a 400 MHz bandwidth avalanche photodetector (APD) for a *phase lock* of the FSR.

A. Absolute frequency lock

About 40 nW of the light transmitted through one of the mirrors is coupled into a wavelength meter to measure the absolute frequency of the light field f_L . At this power, 4 s of integration time are needed per data point, limiting the locking bandwidth to 0.25 Hz. With a resolution of 0.1 MHz and an accuracy of about 2 MHz, the measured value is transferred to a digital proportional-integral-derivative (PID) controller module. A high voltage amplifier drives the piezo actuator and amplifies the PID output by a factor of ten.

B. FSR phase lock

The width of the gain profile of the helium-neon laser is about 1.8 GHz and allows the laser to run on a multitude of longitudinal modes, each of them spaced by one FSR (about 21.4 MHz). The number of active modes increases with the driving power, and the driving power can be adjusted such that the helium-neon plasma lases only on one single mode. Here, we set the driving

power to a slightly higher value, such that small additional modes appear. While modes close to the main carrier are completely suppressed, a secondary mode at $4 \cdot f_{\text{FSR}} = 85.6928$ MHz appears. All higher modes are at least 10 dB weaker.

About 120 nW are available on a high-bandwidth APD. The beat signal at $4 \cdot f_{\text{FSR}}$ has a level of -62 dBm and requires significant filtering and amplification. Good results are achieved by sharp low and high pass filtering of the signal, subsequent amplification with a combination of two amplifiers, and a second set of filters. The combination of a high pass filter with a 1 dB pass band above 90 MHz and a low pass filter with a 1 dB pass band below 81 MHz lead to a combined attenuation of 2.5 dB at the signal frequency, but result in a drastic improvement of the signal-to-noise ratio by several orders of magnitudes. Amplification is done by an extremely low noise figure (NF: 1 dB, gain: 23 dB) amplifier followed by a high-gain amplifier (NF: 6 dB, gain: 34 dB). The resulting signal, together with a highly stable RF signal derived from a synthesizer that is referenced to an atomic clock, are input into a phase detector. The output of that phase detector is a DC voltage proportional to the phase difference of both inputs. This voltage is stabilized by a PID controller that steers the piezo actuator via a high voltage amplifier and thus stabilizes the FSR. Recalling that $f_{\text{FSR}} = c/P$, it is clear that any lock of the FSR also locks the perimeter P and the wavelength λ and thus stabilizes the scale factor.

The bandwidth of this locking scheme is limited to below about 17 Hz by the relatively large inert mass moved by the piezo. A more lightweight setup, where only the mirror is moved by a ring piezo instead of the entire stainless steel mirror mount could increase the bandwidth further into the acoustic regime, at the cost of worse access to the transmitted beams.

III. RESULTS

To evaluate the performance of the *absolute frequency lock* and the *FSR phase lock* in comparison to an unlocked ring laser, we performed three four-hour measurements during consecutive nights, each starting at 11 pm. The absolute lasing frequency f_L , the free spectral range f_{FSR} , and the Sagnac frequency δf are logged during these measurement intervals.

The absolute lasing frequency was constantly measured by the wavelength meter in 4 s intervals, as shown in Fig. 2 a). Without locking, the frequency f_L drifts rather linearly at a rate of 25 MHz h⁻¹. Furthermore, five discontinuities can be observed, which are caused by hopping of the laser mode due to drifting of the laser frequency by more than one FSR. Mode jumps by two FSR are observed as well. Both locking schemes work very well at canceling drifting and therefore also suppress mode hops. In direct comparison, the *FSR phase lock* shows less variation with a standard deviation of f_L of 196 kHz,

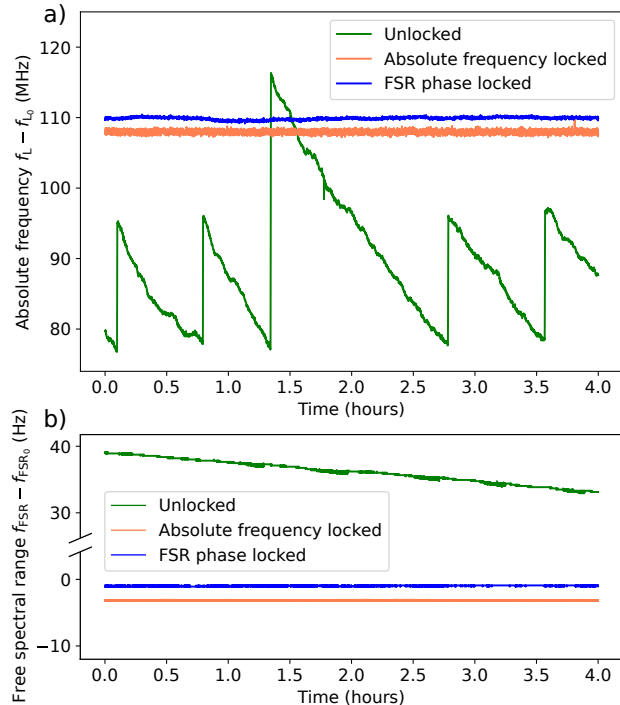


Figure 2. a) Absolute frequency of the ring laser f_L , shifted by $f_{L_0} = 473.612$ THz, as measured by the wavelength meter with a rate of 0.25 Hz for unlocked operation and both locking schemes. b) Beat of the free spectral range f_{FSR} , shifted by $f_{FSR_0} = 21.4232$ MHz, for unlocked operation and both locking schemes.

compared to 334 kHz in the *absolute frequency lock* case, likely caused by the rather slow locking bandwidth due to the long required integration time. Interpreting these deviation values as fluctuations of the $P = 14$ m perimeter yield $\Delta P = 5.8$ nm and 9.9 nm, respectively. Furthermore, using a directional coupler, a 20 dB attenuated part of the amplified and filtered $4 \cdot f_{FSR}$ beat signal is constantly monitored as the peak position in a spectrum analyzer sweep at a rate of 1 Hz with 0.18 Hz resolution, referenced to an atomic clock. Similarly to f_L , an approximately linear downward trend of 1.5 Hz h^{-1} is observed in unlocked operation, as shown in Fig. 2 b). When operating the ring laser using any of the two locking schemes, the measured value of f_{FSR} fluctuates between two 0.18-Hz increments of the spectrum analyzer's resolution.

A datalogger, referenced to an atomic clock, is used to digitize the Sagnac beat signal δf at a sampling rate of 7 kHz, and its frequency is estimated following Ref. [19], as shown in Fig. 3. In unlocked operation, the time series is characterized by drifts and discontinuous jumps of δf , far larger than expected from geometric changes in the scale factor. The cause of these discontinuities are changes in laser dynamics, in particular a near-instantaneous change of backscatter coupling amplitudes,

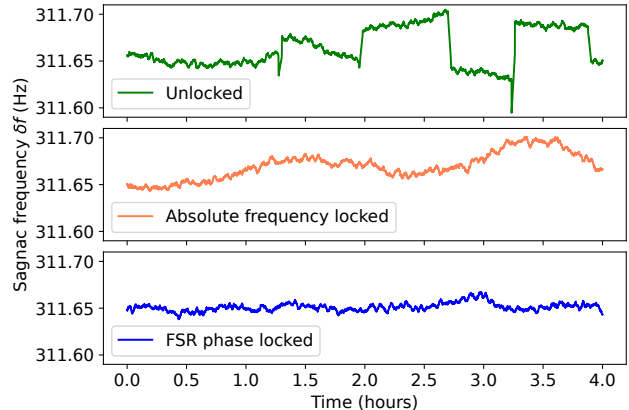


Figure 3. Sagnac frequency δf , plotted with a running mean average of 100 s interval length.

which are likely to happen in a unlocked drifting system with varying lasing frequency f_L and mode index m . Stabilizing the perimeter by either one of the locking schemes drastically reduces the likelihood of discontinuous jumps to the point that none were observed during this measurement.

The *FSR phase lock* reduces residual drifts in δf the best. One origin for the residual variations in δf is laser dynamics that can be accounted for by a backscatter correction [20] and a null-shift correction [21, 22], which are on our current agenda. Another origin is local tilt and beamwander, which will also be detected and corrected for in future improvements.

To quantify the overall performance of the ring laser, Allan deviations of the measured Sagnac signals are calculated according to Ref. [23, 24], see Fig. 4. During *FSR phase locked* operation, the best stability and sensitivity are observed with 280 prad s^{-1} at 250 s integration time, corresponding to $5 \times 10^{-6} \Omega_E$.

IV. CONCLUSION

We have presented two cost-effective and easy-to-implement methods that allow for the stabilization of the perimeter of a large ring laser at the level of a few parts in 10^{-10} . Acknowledging that the current best ring lasers reach a stability of order 10^{-9} in δf , we conclude that the performance of heterolithic ring lasers will not be limited by variations of the perimeter. In the next step, we will also stabilize the beam path using position-sensitive detectors and piezo actuators on the mirrors.

ACKNOWLEDGMENTS

We are indebted to U. Hugentobler and the Forschungseinrichtung Satellitengeodäsie at TU Munich for the

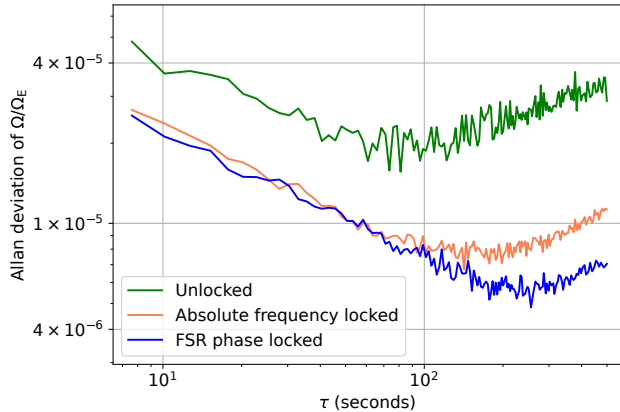


Figure 4. Classic Allan deviations of the measured Sagnac frequency time series shown in Fig. 3. The data is normalized to Earth’s rotation rate Ω_E according to Eq. 1.

loan of the ring laser hardware. We acknowledge fruitful

discussions with J. Kodet, H. Igel, and A. Brotzer, as well as experimental support from P. Hänisch.

DATA AVAILABILITY STATEMENT

The data that support the findings of this study are available from the corresponding author upon reasonable request.

DISCLOSURES

The authors declare no conflicts of interest.

FUNDING

We acknowledge financial support from the European Research Council through grant No. 101123334.

-
- [1] A. A. Michelson, *Astrophysical Journal* **61**, 137 (1925).
- [2] A. A. Michelson and H. G. Gale, *Astrophysical Journal* **61**, 140 (1925).
- [3] G. Sagnac, *Comptes Rendus* **157**, 1410 (1913).
- [4] K. U. Schreiber and J.-P. R. Wells, *Rev. Sci. Instrum.* **84**, 041101 (2013).
- [5] A. Gebauer, M. Tercjak, K. U. Schreiber, H. Igel, J. Kodet, U. Hugentobler, J. Wassermann, F. Bernauer, C.-J. Lin, S. Donner, S. Egdorf, A. Simonelli, and J.-P. R. Wells, *Phys. Rev. Lett.* **125**, 033605 (2020).
- [6] H. Igel, U. Schreiber, A. Flaws, B. Schubert, A. Velikoseltsev, and A. Cochard, *Geophysical Research Letters* **32** (2005).
- [7] H. Igel, M.-F. Nader, D. Kurrle, A. M. G. Ferreira, J. Wassermann, and K. U. Schreiber, *Geophysical Research Letters* **38** (2011).
- [8] G. E. Stedman, *Reports on Progress in Physics* **60**, 615 (1997).
- [9] F. Bosi, G. Cella, A. Di Virgilio, A. Ortolan, A. Porzio, S. Solimeno, M. Cerdonio, J. P. Zendri, M. Allegrini, J. Belfi, N. Beverini, B. Bouhadef, G. Carelli, I. Ferrante, E. Maccioni, R. Passaquieti, F. Stefani, M. L. Ruggiero, A. Tartaglia, K. U. Schreiber, A. Gebauer, and J.-P. R. Wells, *Phys. Rev. D* **84**, 122002 (2011).
- [10] S. Ezekiel and S. R. Balsamo, *Applied Physics Letters* **30**, 478 (1977).
- [11] K. Liu, F. L. Zhang, Z. Y. Li, X. H. Feng, K. Li, Z. H. Lu, K. U. Schreiber, J. Luo, and J. Zhang, *Optics Letters* **44**, 2732 (2019).
- [12] W. Z. Korth, A. Heptonstall, E. D. Hall, K. Arai, E. K. Gustafson, and R. X. Adhikari, *Class. Quantum Grav.* **33**, 035004 (2016).
- [13] K. U. Schreiber, T. Klügel, and G. E. Stedman, *Journal of Geophysical Research: Solid Earth* **108** (2003), <https://agupubs.onlinelibrary.wiley.com/doi/pdf/10.1029/2001JB000569>.
- [14] K. U. Schreiber, J. Kodet, U. Hugentobler, J. Kodet, T. Klügel, and J.-P. R. Wells, *Nat. Photon.* **17**, 1054 (2023).
- [15] F. Zhang, K. Liu, Z. Li, X. Feng, K. Li, Y. Ye, Y. Sun, L. He, K. U. Schreiber, J. Luo, Z. Lu, and J. Zhang, *Class. Quantum Grav.* **37**, 215008 (2020).
- [16] K. U. Schreiber, J. N. Hautmann, A. Velikoseltsev, J. Wassermann, H. Igel, J. Otero, F. Vernon, and J.-P. R. Wells, *Bulletin of the Seismological Society of America* **99**, 1190 (2009).
- [17] U. Schreiber, H. Igel, A. Cochard, A. Velikoseltsev, A. Flaws, B. Schubert, W. Drewitz, and F. Müller, *The geosensor project: Rotations — a new observable for seismology, in Observation of the Earth System from Space* (Springer Berlin Heidelberg, Berlin, Heidelberg, 2006) pp. 427–443.
- [18] R. B. Hurst, M. Mayerbacher, A. Gebauer, K. U. Schreiber, and J.-P. R. Wells, *Applied Optics* **56**, 1124 (2017).
- [19] H. Igel, K. U. Schreiber, A. Gebauer, F. Bernauer, S. Egdorf, A. Simonelli, C.-J. Lin, J. Wassermann, S. Donner, C. Hadziioannou, S. Yuan, A. Brotzer, J. Kodet, T. Tanimoto, U. Hugentobler, and J.-P. R. Wells, *Geophysical Journal International* **225**, 684 (2021), <https://academic.oup.com/gji/article-pdf/225/1/684/36262043/ggaa614.pdf>.
- [20] R. B. Hurst, N. Rabeendran, K. U. Schreiber, and J.-P. R. Wells, *Applied Optics* **53**, 7610 (2014).
- [21] A. Beghi, J. Belfi, N. Beverini, N. Bouhadef, D. Cuccato, A. Di Virgilio, and A. Ortolan, *Applied Optics* **51**, 7518 (2012).
- [22] A. D. V. Di Virgilio, N. Beverini, G. Carelli, D. Ciampini, F. Fusco, and E. Maccioni, *Eur. Phys. J. D* **79**, 573 (2019).
- [23] D. Allan, *Proceedings of the IEEE* **54**, 221 (1966).

- [24] D. Sullivan, D. Allan, D. Howe, and F. Walls, NASA STI/Recon Technical Report N **1337** (1990).